A

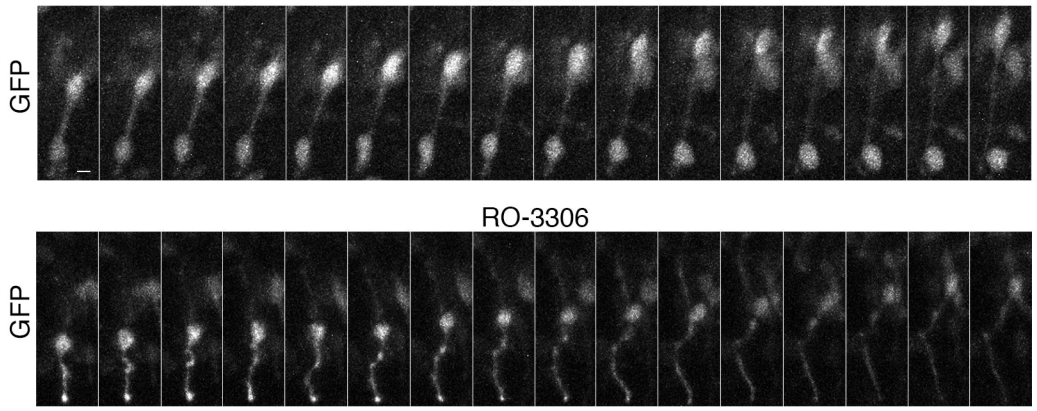
Roscovitine
GFP
RO-3306
GFP

C

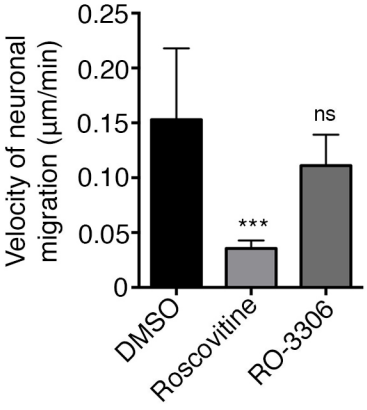
Velocity of neuronal migration (µm/min)
0.25
0.20
0.15
0.10
0.05
0
***
ns
DMSO
Roscovitine
RO-3306

B

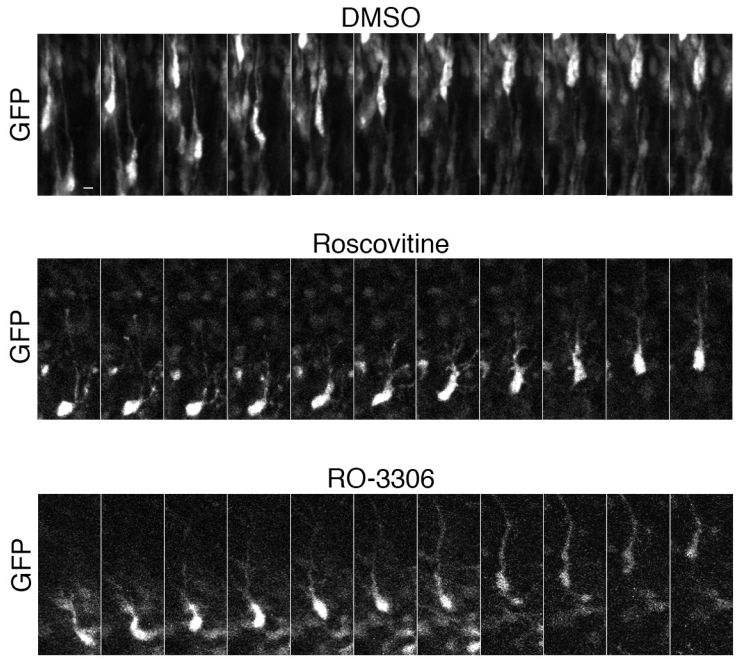
DMSO
GFP
Roscovitine
GFP
RO-3306
GFP

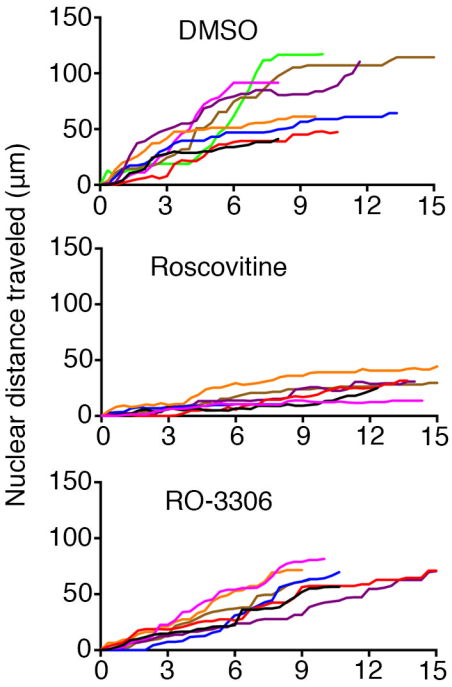
Nuclear distance traveled (µm)
DMSO
Roscovitine
RO-3306
150
100
50
0
0
3
6
9
12
15

Figure S2

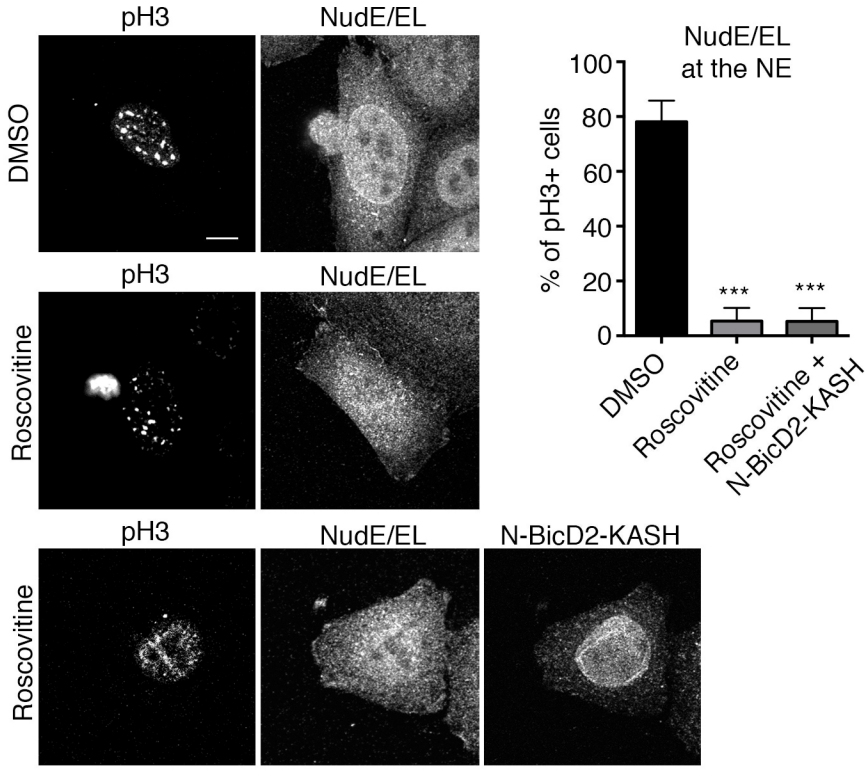
pH3
NudE/EL
DMSO
pH3
NudE/EL
Roscovitine
pH3
NudE/EL
N-BicD2-KASH
Roscovitine
NudE/EL
at the NE
% of pH3+ cells
100
80
60
40
20
0
***
***
DMSO
Roscovitine
Roscovitine +
N-BicD2-KASH

Figure S3

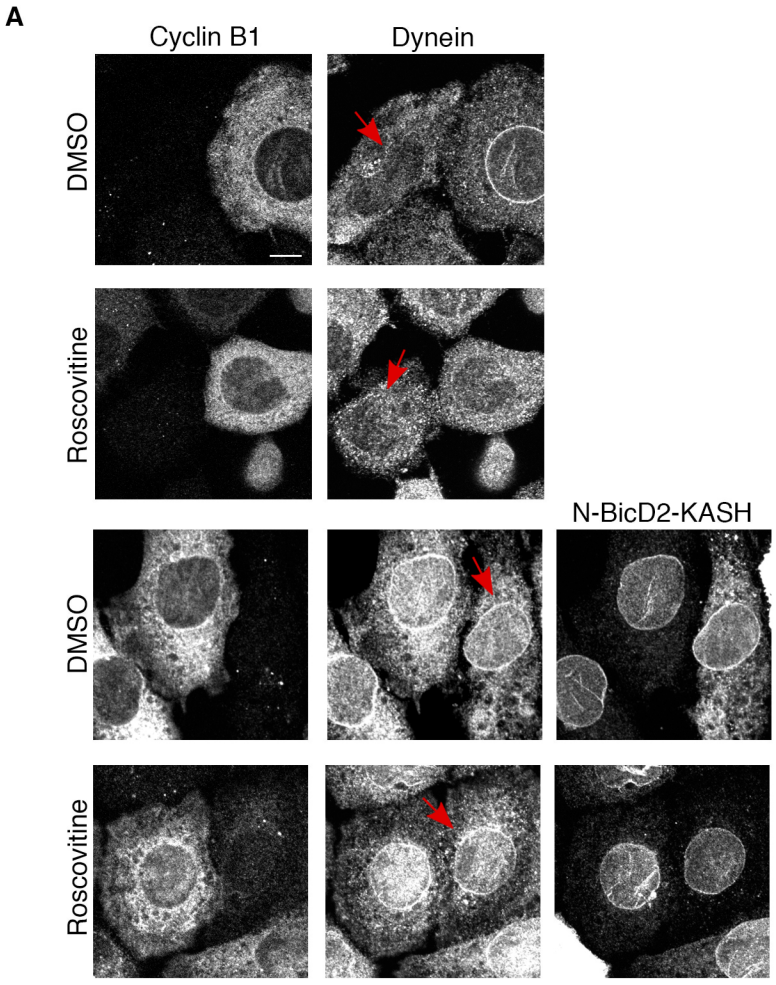
A
Cyclin B1
Dynein
DMSO
Roscovitine
N-BicD2-KASH
DMSO
Roscovitine

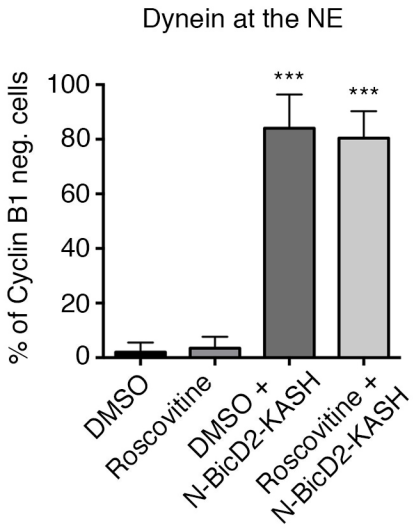
Dynein at the NE
% of Cyclin B1 neg. cells
100
80
60
40
20
0
***
***
DMSO
Roscovitine
DMSO + N-BicD2-KASH
Roscovitine + N-BicD2-KASH

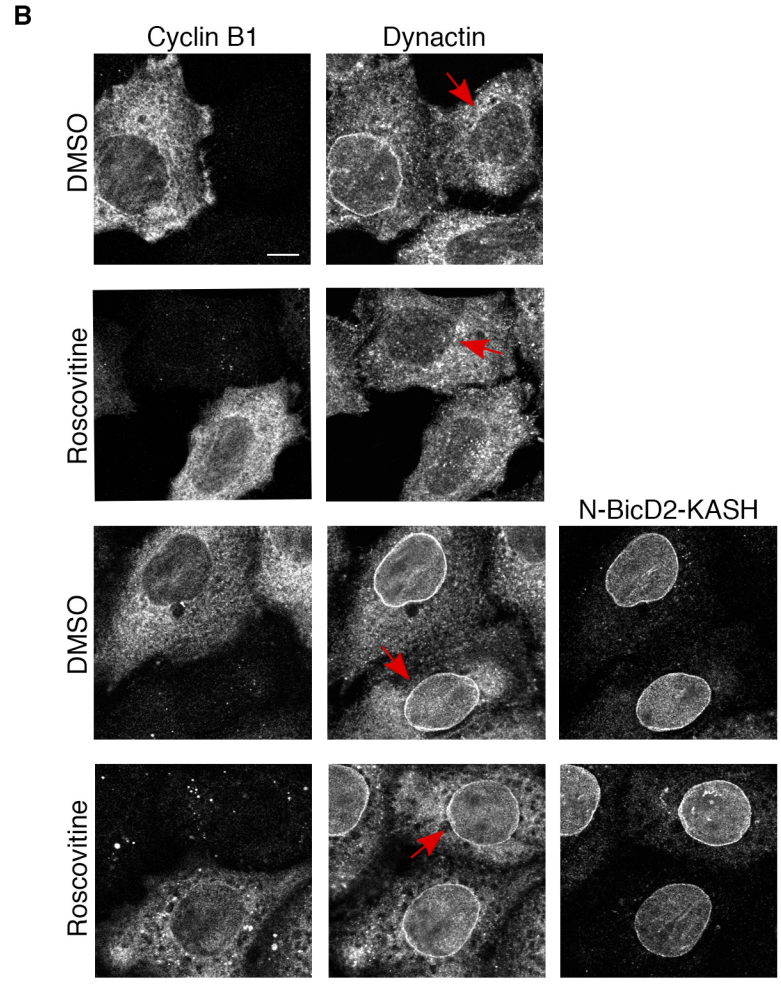
B
Cyclin B1
Dynactin
DMSO
Roscovitine
N-BicD2-KASH
DMSO
Roscovitine

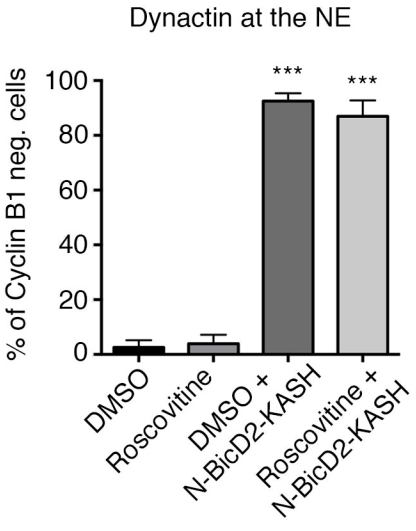
Dynactin at the NE
% of Cyclin B1 neg. cells
100
80
60
40
20
0
***
***
DMSO
Roscovitine
DMSO + N-BicD2-KASH
Roscovitine + N-BicD2-KASH

A

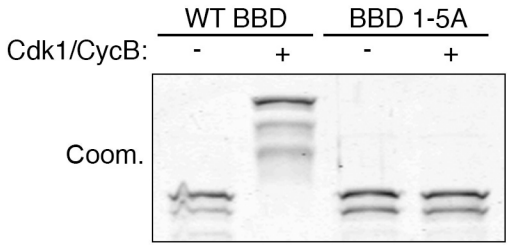
WT BBD
BBD 1-5A
Cdk1/CycB:
-
+
-
+
Coom.

B

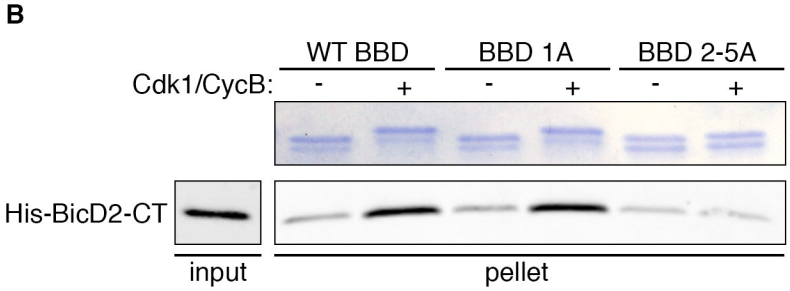
WT BBD
BBD 1A
BBD 2-5A
Cdk1/CycB:
-
+
-
+
-
+
His-BicD2-CT
input
pellet

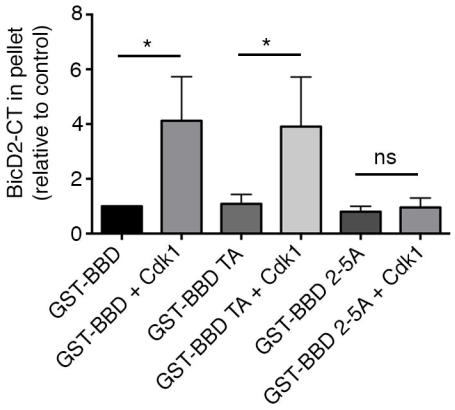
BicD2-CT in pellet
(relative to control)
8
6
4
2
0
*
*
ns
GST-BBD
GST-BBD + Cdk1
GST-BBD TA
GST-BBD TA + Cdk1
GST-BBD 2-5A
GST-BBD 2-5A + Cdk1

A

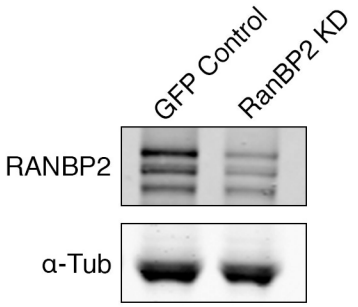
GFP Control
RanBP2 KD
RANBP2
α-Tub

C

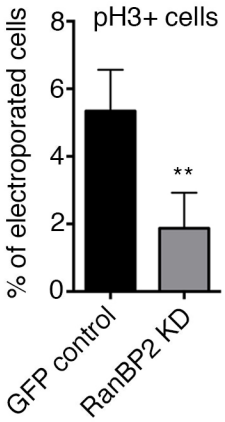
pH3+ cells
% of electroporated cells
8
6
4
2
0
**
GFP control
RanBP2 KD

B

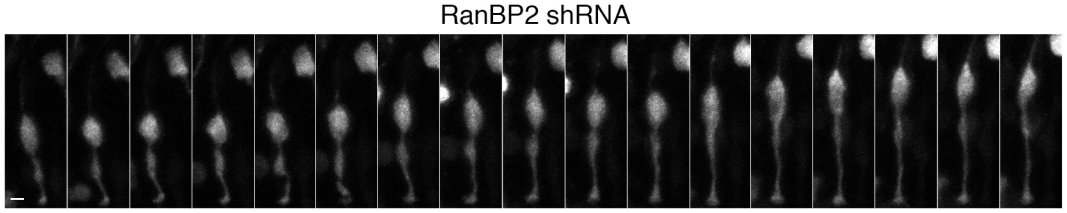
RanBP2 shRNA
30 minutes interval

Supplemental Information

Supplemental figure legends

Figure S1. Effect of Cdk1 inhibitors on basal nuclear migration in RGPs and on neuronal migration, Related to Figure 1

(A) Live imaging of GFP-electroporated RGP cells undergoing basal nuclear migration and treated with Roscovitine (55 μM) or RO-3306 (100 μM). This movement is not significantly affected by Roscovitine or RO-3306 treatment. (B) Live imaging of GFP-electroporated bipolar neurons undergoing radial migration and treated with Roscovitine (55 μM) or RO-3306 (100 μM). Neurons were imaged in the intermediate zone (IZ) and cortical plate (CP). Right: representative tracks. RO-3306-treated neurons are not significantly affected, as compared to DMSO-treated neurons (control). Roscovitine-treated neurons migrate significantly slower, consistent with inhibition of Cdk5. (C) Quantification of neuronal migration speed for each indicated condition. For each experiment, at least three independent brains were imaged. Error bars indicate SD; ***$p<0.001$; ns = not significant, based on a Student's t-test. Scale bar, 5 μm.

Figure S2. Forced recruitment of BicD2 to the NE does not rescue NudE/EL localization in Cdk1-inhibited cells, Related to Figure 5

HeLA cells stained for pH3 and NudE/EL. In DMSO-treated cells (control), NudE/EL localizes to the NE of 78.1 ± 7.7% of pH3+ cells. After 30 minutes treatment with

Roscovitine (55 μM), NudE/EL is displaced and only localizes to 5.4 ± 4.8% of pH3+ cells. BicD2-N-KASH overexpression in Roscovitine-treated cells does not restore perinuclear NudE/EL accumulation (5.2 ± 4.9%). Each experiment was reproduced three independent times (over 50 cells per condition and per experiment were counted). Error bars indicate SD; ***p<0.001, based on a Student's t-test. Scale bar, 10 μm.

Figure S3. N-BicD2-KASH induces dynein/dynactin recruitment to the NE of Cyclin B1 negative cells, Related to Figure 5

(A-B) Effect of N-BicD2-KASH expression on recruitment of (A) dynein and (B) dynactin to the NE of Cyclin B1 negative cells (+/- Roscovitine, 55 μM, 30 minutes). Unlike untransfected cells, Cyclin B1 negative cells (indicated by red arrows) expressing N-BicD2-KASH display perinulear dynein and dynactin staining, even after Roscovitine treatment. Each experiment was reproduced three independent times (over 50 cells per condition and per experiment were counted). Error bars indicate SD; ***p<0.001, based on a Student's t-test. Scale bar, 10 μm.

Figure S4. A cluster of serine residues in RanBP2 regulates Cdk1-dependent interaction with BicD2, Related to Figure 6

(A) *In vitro* Cdk1 phosphorylation of GST-BBD WT and mutated to alanine in all five identified Cdk1 phosphorylation sites (GST-BBD 1-5A). Proteins were analyzed on Coomassie-stained phosphate binding tag (Phos-Tag)-containing gels. The strong electrophoretic gel shift observed for the WT fragment was abolished in the BBD 1-

5A fragment. (B) GST-pull down assay with indicated RanBP2 fusions and purified His-BicD2-CT in the presence or absence of purified Cdk1 + Cyclin B. 10% of the input and 50% of the bound fraction were loaded on gel. Right: Quantification of BicD2-CT bound fraction relative to amount bound to GST-BBD (n=3 independent experiments). Pull down with GST-BBD 2-5A (all four serines mutated to alanines) shows loss of Cdk1-dependant affinity increase for BicD2-CT. Pull down with GST-BBD 1A (threonine mutated to alanine) has no effect. Error bars indicate SD; *p<0.05; ns = not significant, based on a Student's t-test.

Figure S5. Validation of RanBP2 knockdown and effect on basal migration and mitotic index, Related to Figure 7

(A) Western Blot analysis of RanBP2 protein levels in C6 rat cells transfected with RanBP2 shRNA construct. (B) Live imaging of RanBP2 shRNA-expressing RGP cell undergoing basal nuclear migration. (C) Quantification of the percentage of pH3+ electroporated cells (mitotic index). RanBP2 knockdown significantly affects mitotic entry, consistent with impaired apical nuclear migration. For each experiment, at least three independent brains were imaged. Error bars indicate SD; **p<0.01, based on a Student's t-test. Scale bar, 5 μm.

Movie S1: Interkinetic nuclear migration in control RGP cell, Related to Figure 1

E16 rat embryonic brain was electroporated with vector expressing GFP. Brain was sectioned at E19 and imaged at 10 min intervals.

Movie S2: Apical nuclear migration arrest of RGP cell treated with Roscovitine, Related to Figure 1

E16 rat embryonic brain was electroporated with vector expressing GFP. Brain was sectioned at E19 and imaged at 10 min intervals in the presence of Roscovitine (55 μM). Nucleus of RGP cell was arrested away from the ventricular surface throughout recording.

Movie S3: Basal nuclear migration in RGP cell treated with Roscovitine, Related to Figure 1

E16 rat embryonic brain was electroporated with vector expressing GFP. Brain was sectioned at E19 and imaged at 10 min intervals in the presence of Roscovitine (55 μM). Nucleus of RGP cell exhibited basal migration.

Movie S4: Apical nuclear migration arrest of RGP cell treated with RO-3306, Related to Figure 1

E16 rat embryonic brain was electroporated with vector expressing GFP. Brain was sectioned at E19 and imaged at 10 min intervals in the presence of RO-3306 (100 μM). Nucleus of RGP cell was arrested away from the ventricular surface throughout recording.

Movie S5: Basal nuclear migration in RGP cell treated with RO-3306, Related to Figure 1

E16 rat embryonic brain was electroporated with vector expressing GFP. Brain was sectioned at E19 and imaged at 10 min intervals in the presence of RO-3306 (100 μM). Nucleus of RGP cell exhibited basal migration.

Movie S6: Apical arrest of RGP cell nucleus after 4 days of RanBP2 RNAi, Related to Figure 6

E16 rat embryonic brain was electroporated with vectors expressing RanPB2 shRNA. Brain was sectioned at E20 and imaged at 10 min intervals. Nucleus of RGP cell was arrested away from the ventricular surface throughout recording.

Movie S7: Basal nuclear migration in RGP cell subjected to 4 days of RanBP2 RNAi, Related to Figure 6

E16 rat embryonic brain was electroporated with vectors expressing RanBP2 shRNA. Brain was sectioned at E20 and imaged at 10 min intervals. Nucleus of RGP cell exhibited basal migration.

Movie S8: Apical nuclear migration arrest of RGP cell expressing wild type BicD2 and treated with Roscovitine, Related to Figure 6

E18 rat embryonic brain was electroporated with vectors expressing wild type BicD2 and GFP. Brain was sectioned at E19 and imaged at 10 min intervals in the

presence of Roscovitine (55 μM). Nucleus of RGP cell was arrested away from the ventricular surface throughout recording.

Movie S9: Apical nuclear migration of RGP cell expressing N-BicD2-KASH and treated with Roscovitine, Related to Figure 6

E18 rat embryonic brain was electroporated with vectors expressing N-BicD2-KASH and DsRed. Brain was sectioned at E19 and imaged at 10 min intervals in the presence of Roscovitine (55 μM). Apical migration of RGP cell nucleus was restored.

Supplemental experimental procedures

Mass spectrometry for identification of Cdk1 phosphorylation sites

The dried gel pieces were rehydrated and digested in 80 μL of 12.5 ng/μL Trypsin Gold/50 mM ammonium bicarbonate at 37 °C overnight. After the digestion was complete, condensed evaporated water was collected from tube walls by brief centrifugation using benchtop microcentrifuge (Eppendorf, Hauppauge, NY). The gel pieces and digestion reaction were mixed with 50 μL 2.5% TFA and rigorously mixed for 15 min. The solution with extracted peptides was transferred into a fresh tube. The remaining peptides were extracted with 80μl 70% ACN/5% TFA mixture using rigorous mixing for 15 min. The extracts were pooled and dried to completion (1.5–2 h) in SpeedVac. The dried peptides were reconstituted in 30 μl 0.1% TFA by mixing for 5 min and stored in ice or at −20 °C prior to analysis.

The concentrated peptide mix was then reconstituted in a solution of 2 % acetonitrile (ACN), 2 % formic acid (FA) for MS analysis. Peptides were loaded with

the autosampler directly onto a 2cm C18 pre-column and were eluted from the column using a Thermo Easy-nLC1000 UHPLC with a 10 min gradient from 2% buffer B to 35 % buffer B (100 % acetonitrile, 0.1 % formic acid). The gradient was switched from 35 % to 85 % buffer B over 1 min and held constant for 2 min. Finally, the gradient was changed from 85 % buffer B to 98 % buffer A (100% water, 0.1% formic acid) over 1 min, and then held constant at 98 % buffer A for 5 more minutes. The application of a 2.0 kV distal voltage electrosprayed the eluting peptides directly into the mass spectrometer equipped with an Easy-spray source (Thermo Finnigan). Mass spectrometer-scanning functions and HPLC gradients were controlled by the Xcalibur data system (Thermo Finnigan, San Jose, CA).

Tandem mass spectra from raw files were searched against a human protein database using the Proteome Discoverer (Thermo Finnigan, San Jose, CA). The Proteome Discoverer application extracts relevant MS/MS spectra from the .raw file and determines the precursor charge state and the quality of the fragmentation spectrum. The Proteome Discoverer probability-based scoring system rates the relevance of the best matches found by the SEQUEST algorithm. The human database was downloaded as FASTA-formatted sequences from Uniprot protein database. The peptide mass search tolerance was set to 10ppm. A minimum sequence length of 7 amino acids residues was required. Only fully tryptic peptides were considered. To calculate confidence levels and false positive rates (FDR), Proteome Discoverer generates a decoy database containing reverse sequences of the non-decoy protein database and performs the search against this concatenated database (non-decoy + decoy). The discriminant score was set at 1% FDR

determined based on the number of accepted decoy database peptides to generate protein lists for this study. The predicted phosphorylation sites were analyzed manually to confirm the precursor mass, fragmentation ions, and phosphorylated amino acids for the predicted phosphopeptides.